Fluid Dynamics & Materials Processing

Tech Science Press

DOI: 10.32604/fdmp.2021.015161

ARTICLE

Effect of Al_2O_3 Nanoparticle on Cavitation Strengthening of Magnesium Alloys

Lei Liu*, Chuanhui Huang, Xinghua Lu, Ping Yu, Longhai Li and Huafeng Guo

Xuzhou Institute of Technology, Xuzhou, 221000, China

*Corresponding Author: Lei Liu. Email: leiliu86@sina.cn

Received: 26 November 2020 Accepted: 01 March 2021

ABSTRACT

In order to study the effect of Al_2O_3 nanoparticles in the cavitation-based strengthening process of magnesium alloys, the impact of a micro-jet generated by bubble collapse has been considered. The strengthening mechanism is based on the transfer of the energy of cavitation due to bubble collapse to Al_2O_3 particles, which then undergo collision with the surface of the sample. The hardness, surface morphology, element content and chemical state of the strengthened samples have been analyzed by microhardness tests, SEM (scanning electron microscopy) and XPS (X-ray photoelectron spectroscopy) techniques. The results show that: after 5 min of strengthening, nanoparticles can be found on the surface of the sample through SEM. Combined with XPS tests, the content of Al_2O_3 in the sample can be significantly increased, indicating that Al_2O_3 particles penetrate into the surface and increase its hardness by 29.1 HV.

KEYWORDS

Cavitation; nanoparticles; strengthening; SEM; XPS

1 Introduction

Magnesium (Mg) is an abundant element in nature. In particular, magnesium is the third abundant element in the Earth's crust. Considering non-pollution, Mg and its alloys are known as environmentally-friendly engineering metals [1]. Although Mg alloys have many superior characteristics, they have some shortcomings, including low absolute strength and hardness [2], and poor wear resistance [3] compared with conventional engineering alloys, thereby limiting their application in numerous industrial fields. Accordingly, investigations to improve the strength and hardness of Mg alloys are of significant importance.

Recently, the strengthening theories and technologies to obtain lightweight alloys have developed rapidly [4–6]. For example, it was found that the surface aluminizing approach is an effective method to improve the corrosion resistance of magnesium alloys [7]. Zhang et al. [8] explored the effect of mechanical shot peening on the fatigue resistance of ZK60 Mg alloy. It should be indicated that the pure cavitation [9] strengthening has a similar principle with the shot peening, through which a better surface quality can be obtained. Further investigations demonstrate that pure cavitation strengthening can better improve the fatigue strength of complex or miniature parts [10]. High-speed micro-jets that are normally generated during pulsation of cavitation bubbles have the same principle as micro-jets, where the water hammer pressure in a flow field is applied to the surface of solid materials to change their surface properties [11,12]. In this regard, Orthaber et al. [13] designed a device to generate cavitation bubbles

through high-speed jets for modifying the material surface. Obtained results showed that high-speed water jets increase the residual compressive stress and improve the mechanical properties of the material surface. From the shot peening point of view, the resulting materials present smoother surface morphologies.

Studies show that morphology, texture, and grain size of the material surface affect the material properties. Accordingly, the mechanical shot peening can be combined with pure cavitation strengthening. In this regard, experiments were conducted on magnesium-aluminum (Mg-Al) alloys, where Al_2O_3 nanoparticles are added in water and then embedded within the samples by the generated energy because of the cavitation-bubble collapse.

2 Test Methods

In this section, experiments were conducted by an ultrasonic cavitation testing machine (SLQS1000, Company name). Fig. 1 shows the test machine in this regard.

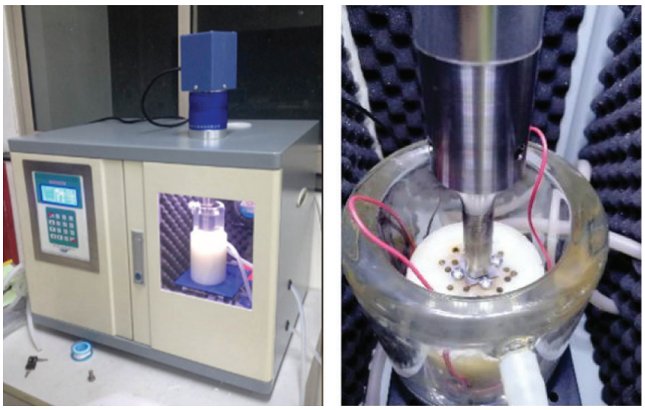

Figure 1: Test equipment

In the experiment, test parameters were set as follows: ultrasonic power of 800 W; ultrasonic frequency of 20 kHz; the amplitude-measuring transformer with a diameter of 15.8 mm at a distance of 0.5 mm to the sample surface; the test temperature was 25°C. Moreover, specimens made of AZ31 Mg alloy and dimensions of 20 mm × 20 mm × 0.2 mm were considered as the research object. The diameter of Al_2O_3 particles was less than 500 nm. Meanwhile, all samples were polished before testing to reach the surface polish of 5000 mesh. After the test, samples were cleaned and dried and then preserved in sealed containers.

In order to perform the experiment, samples were put in a water solution, and then Al_2O_3 nanoparticles were added to the water. Then the mixture was stirred evenly through ultrasonic-induced cavitation until bubbles collapsed near the sample wall, which originated from micro-jet Al_2O_3 particles at a certain energy impact samples and infiltration of the surface. This process realizes the increment of surface hardness.

The samples were characterized and tested by applying a scanning electron microscope (SEM) (F50, FEI Inspect), an X-ray photoelectron spectrometer (XPS) (250Xi, Thermo Fisher EscaLab), and a Vickers hardness tester. Variations of different parameters, including the surface morphology, chemical state, and microhardness of the samples were monitored.

3 Results and Discussion

3.1 The Influence of the Treatment Mode

In order to analyze the influence of Al_2O_3 particles on the strengthening process, compared with the pure cavitation strengthening (i.e., strengthening without Al_2O_3 particles). Fig. 2 shows the surface morphology of the sample after 5 min of action.

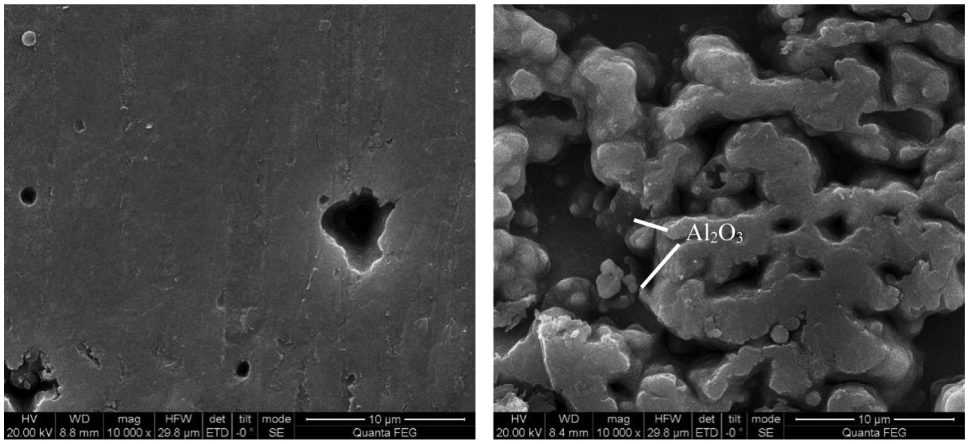

(a) (b)

Figure 2: Surface morphologies of the samples after being treated for 5 min through different strengthening methods (a) pure cavitation strengthening: without Al_2O_3 particles (b) coupled strengthening: with Al_2O_3 particles

Fig. 2a indicates that in the pure cavitation strengthening mode without Al_2O_3 particles, 1 μm–4 μm diameter pits appear on the surface of the sample.

These mechanisms originate from the micro-jet impact generated by the cavitation bubble collapse. In the initial stage, slight deformation appears at the point subjected to the micro-jet impact on the sample surface and shear failure is gradually generated at the edge so that erosion pits appear. Moreover, considering micro-jets differing in the impact direction and intensity, certain positions on the sample surface are more deformed so that the pitting diameter differs greatly. Fig. 3 schematically presents the micro-jet impact.

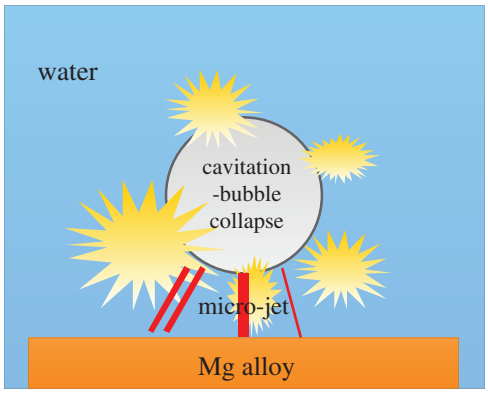

Figure 3: Schematic diagram of the micro-jet impact

Fig. 2b indicates that after 5 min of coupled strengthening with Al_2O_3 particle, the surface morphology of the sample changes greatly. Under this circumstance, more pits appeared and some pits are gradually connected. Therefore, a smooth edge is achieved. Meanwhile, it is found that particles smaller than 500 nm exist in the pit, indicating that Al_2O_3 particles infiltrate into the sample surface. In this case, the strengthening mechanism can be described by impacts of Al_2O_3 particles on the sample surface rather than cavitation bubble collapse energy being directly applied to the samples. Therefore, a lower impact

force is imposed on the particle, and the transition zone a continuous and smooth pit is achieved. This issue is of significant importance to prevent unwanted deformation through micro-cracks and sharp edges [14]. Furthermore, Al_2O_3 nanoparticles have a reasonable hardness and a better strengthening effect after embedding within the sample surface.

In order to prove the infiltration of Al_2O_3 particles and analyze the changes in the chemical state of elements, the XPS full-spectrum, high-resolution spectrum of Mg1s and Al2p of the sample under two strengthening methods are shown in Fig. 4.

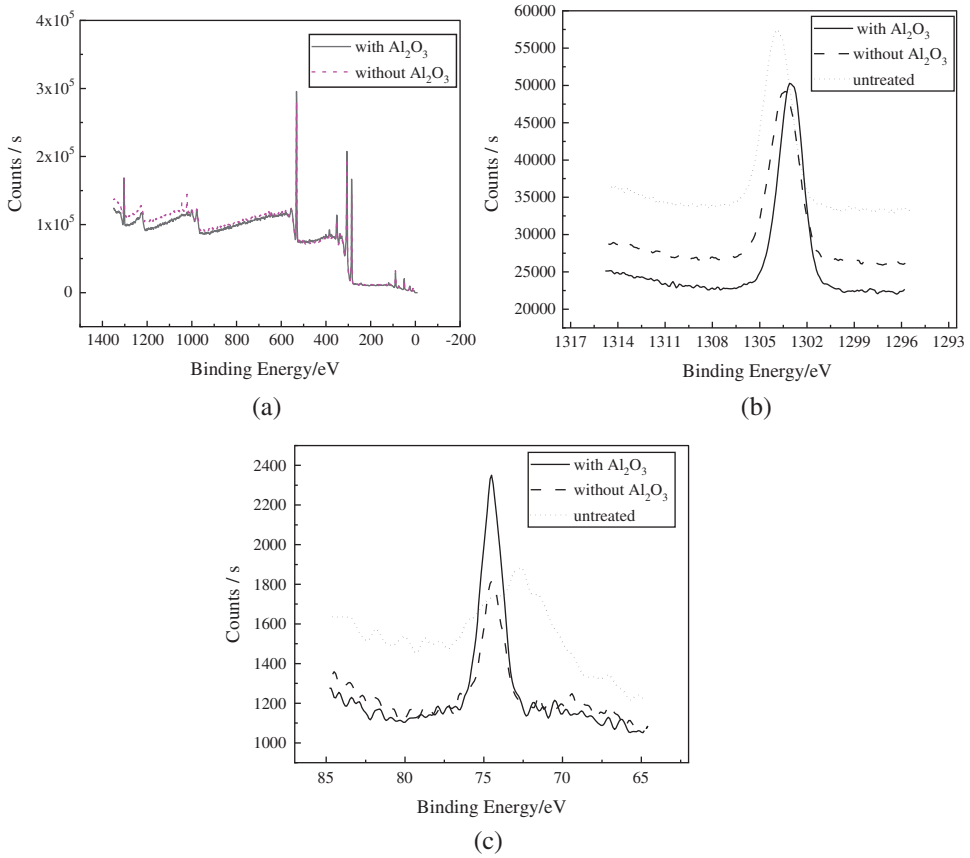

Figure 4: High-resolution XPS spectra (a) full spectrum (b) Mg1s (c) Al2p

Fig. 4a shows that regardless of the presence of Al_2O_3 particles, the position of the main peak of the two strengthening methods does not change significantly after 5 min of action. Therefore, the composition of the substance is the same.

Moreover, Fig. 4b shows that the binding energy of the element Mg at the peak value after the coupled strengthening with Al_2O_3 particles is 1303.1 eV, which corresponds to metal Mg according to previous research [15]. Furthermore, the binding energy at the peak value after the pure cavitation strengthening without Al_2O_3 particles is 1303.6 eV, which also corresponds to the metallic Mg. The peak of the original samples obtains binding energy of 1303.9 eV, which corresponds to MgO. This is because the metal Mg on the sample surface is exposed to air for a long time and oxidized to MgO before the strengthening tests. Therefore, both modes of strengthening change the surface morphologies and exfoliate the MgO from the original surface, while exposing metal Mg at greater depth.

Fig. 4c illustrates that the binding energies of Al elements in the samples under the two strengthening methods appear at the same position, indicating similar compositions. However, the peak intensity between them differs significantly. It is found that the peak value under the coupled strengthening with Al_2O_3 particles is higher than that under pure cavitation strengthening without Al_2O_3 particles. The specific parameters are as follows: The Al2p peak of the original samples corresponds to the binding energy of 72.7 eV, mainly denoted as metallic Al. After the pure cavitation strengthening without Al_2O_3 particles, the peak shifts to the position of high binding energy at 74.5 eV. This implies that the metallic Al is transformed into Al^{3+} in the form of Al_2O_3 due to the loss of electrons, which is attributed to the released heat during the cavitation bubble collapse. Therefore, considering the original samples, the binding energy varies, while the strength of the samples remains practically unchanged after pure cavitation strengthening without Al_2O_3 particles treatment. This indicates that the valence state of Al elements changes, while their content remains unchanged. After coupled strengthening with Al_2O_3 particles, the peak also appears at 74.5 eV, while there is larger binding energy. This indicates that Al_2O_3 particles in the solution are embedded within the samples adjunct to the metal Al being transformed into Al_2O_3 under the effect of heat release during cavitation bubble collapse. Therefore, Tab. 1 shows that the elemental Al content increases.

Table 1: The proportional elemental Al content

Treatment mode	Original	Without Al_2O_3 particles	With Al_2O_3 particles
Content	2.36%	2.33%	3.4%

Fig. 5 shows that in order to determine the specific chemical state of the elemental Al, peak fitting is applied to the XPS curves of Al2p.

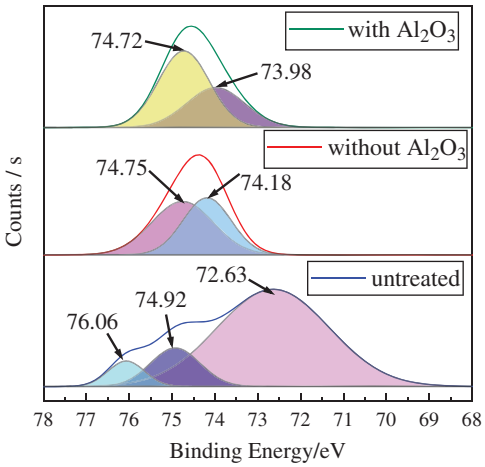

Figure 5: Peak fitting curves: Al2p

It is observed that there are three peaks in the original samples at 72.63 eV, 74.92 eV, and 76.06 eV, corresponding to Al, Al_2O_3, and Al_2O_3/A1. Two peaks appear in the samples after pure cavitation strengthening without Al_2O_3 particles at 74.18 eV and 74.75 eV. Moreover, two peaks occur in the samples after the coupled strengthening with Al_2O_3 particles at 73.98 eV and 74.72 eV, both corresponding to Al_2O_3.

The A12p binding energy of the aluminum-oxide tetrahedron [AlO_4] and the aluminum-oxide octahedron [AlO_6] are about 73.8 eV ± 0.4 eV and 74.5 ± 0.4 [16], respectively. However, Fig. 5 shows

that the sub-peaks of Al2p under two strengthening modes are located within the abovementioned ranges. This indicates that Al in the samples after being subjected to the two strengthening treatments appear as Al_2O_3. However, they show different coordination modes. Tab. 2 presents the comparison of the surface hardness.

Table 2: Vickers hardness/HV

Original	Without Al_2O_3 particles	With Al_2O_3 particles
80.2	91.6	109.3

It can be found that the surface hardness of Mg alloy, after cavitation strengthening without Al_2O_3 particles for 5 min, increased by 11.4 HV and by 29.1 HV after coupled strengthening with Al_2O_3 particles. This indicates that the addition of Al_2O_3 particles greatly enhances the strengthening effect.

3.2 The Influence of the Treatment Duration

The sample surface undergoes damage after 10 min. In this case, the binding capacity between Al_2O_3 particles and the surface layer of the samples decreases. Moreover, Fig. 6 shows that most of the particles are gradually exfoliated from the sample surface.

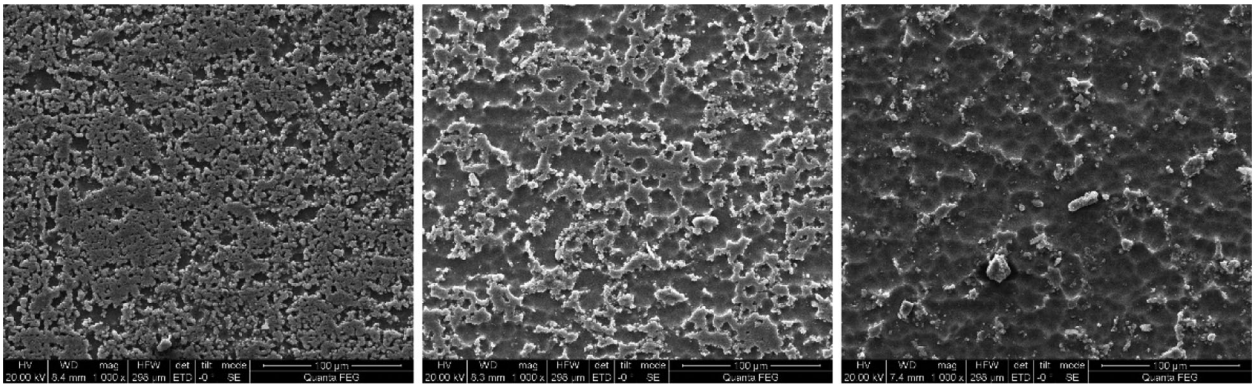

(a) (b) (c)

Figure 6: Comparison of the surface morphology of samples by different strengthening times (a) 10 min (b) 15 min (c) 20 min

As the action time increases, the sample undergoes cavitation erosion. As a result, the embedded Al_2O_3 particles are released from the surface. Therefore, the content of Al_2O_3 in the sample significantly decreases and becomes equivalent to the content of Al_2O_3 under pure cavitation strengthening without Al_2O_3 particles. This indicates that Al_2O_3 particles are released from the surface of the sample and the chemical state of the Al element gradually becomes similar to that of pure cavitation, as shown in Fig. 7.

Fig. 7 illustrates that the binding energy of the Al element in the samples under the two functional models appears in a similar position as the treatment duration changes. This shows that the same chemical state exists in different treatment durations. After being treated for 10 to 15 min, the peak amplitude decreases and the Al^{3+} content decreases to a significant extent. This is mainly due to the morphological damage of the Al_2O_3 particles, which are separated from the sample. After treatment for 15 to 20 min, the peak value under the pure cavitation strengthening effect is higher than that under the coupled strengthening effect. However, Tab. 3 shows that the difference between them is not significant.

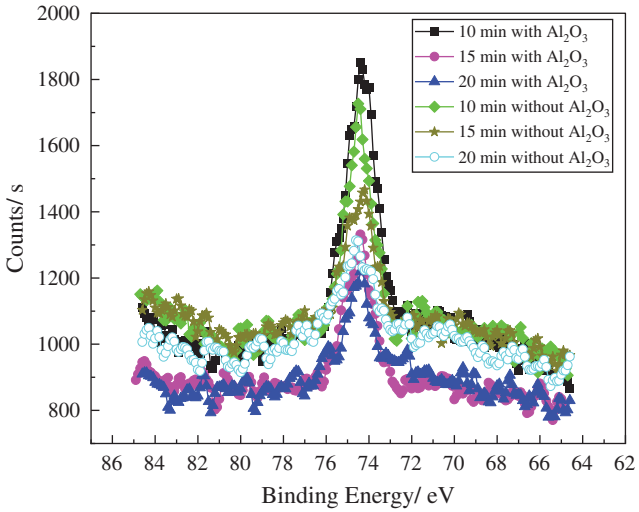

Figure 7: XPS spectra of Al2p treated for different durations

Table 3: The proportional elemental Al content after treatment for different durations

Time	10 min	15 min	20 min
With Al_2O_3 particles	3.82%	2.43%	2.41%
Without Al_2O_3 particles	2.73%	2.6%	2.53%

Fig. 8 shows the changes in the microhardness of samples in different treatment durations.

It is observed that the strengthening effect of the two modes of treatment on the specimens conforms to the Gaussian distribution, which is expressed as follows: the optimal strengthening effect appears within 5 to 10 min. Then, the rate of the reduction of the microhardness increases under the effects of the coupled strengthening with Al_2O_3 particles. This indicates that the microhardness is related to the morphology of the specimen and the amount of Al_2O_3 particles.

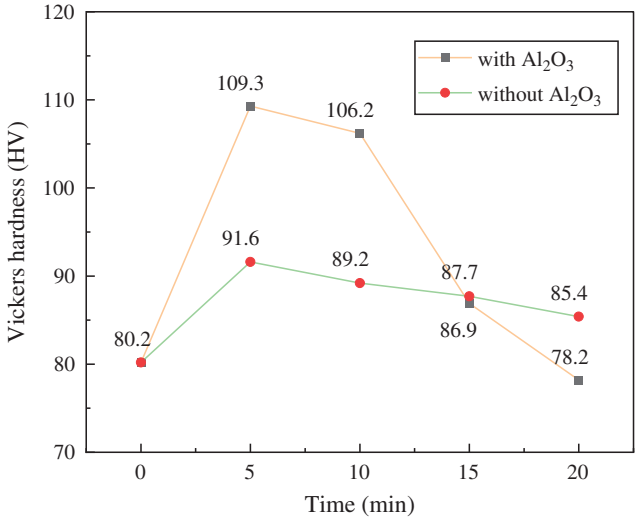

Figure 8: The changes in the microhardness with different treatment durations

4 Conclusion

Obtained results show that cavitation bubbles collapse near the sample wall, Al_2O_3 particles under the action of micro-jet infiltration of the magnesium alloy surface, realize the reinforcement, and as the growth of the time to produce cavitation damage, Al_2O_3 particles leave from the surface. The experiments show that compared with the pure cavitation strengthening method, in the proposed method, Al_2O_3 particles penetrate the surface to improve the performance of the main factors. Therefore, the oxidation state of the Al content is significantly higher, and the surface hardness increases significantly.

Funding Statement: This work is supported by the University Natural Science Research Programme of Jiangsu Province (Grant No. 18KJB460028), Project of Xuzhou University of Technology (Grant No. XKY2019215), the Natural Science Foundation of Jiangsu Province (Grant No. BK20180177), and the Xuzhou Science & Technology Project (Grant No. KC18014).

Conflicts of Interest: The authors declare that they have no conflicts of interest to report regarding the present study.

References

1. Akinwamide, S. O., Lemika, S. M., Obadele, B. A., Akinribide, O. J., Abe, B. T. et al. (2019). A study on microstructural and mechanical properties of a Stir Cast Al (SiC-Mg-TiFe) composite. *Fluid Dynamics & Materials Processing, 15(1),* 15–26. DOI 10.32604/fdmp.2019.04761.
2. Ding, W. J. (2007). *Magnesium alloy science and technology.* Beijing: Science Press.
3. Zhang, A. M., Quan, G. F. (2010). Prospect and research progress of fatigue properties of magnesium alloys. *Materials for Mechanical Engineering, 34(5),* 1–4.
4. Luo, X. C., Zhang, D. T., Cao, G. H., Qiu, C., Chen, D. L. (2019). Multi-pass submerged friction stir processing of AZ61 magnesium alloy: Strengthening mechanisms and fracture behavior. *Journal of Materials Science, 54(11),* 8640–8654. DOI 10.1007/s10853-018-03259-w.
5. Straumal, B. B., Pontikis, V., Kilmametov, A. R., Mazilkin, A. A., Dobatkin, S. V. et al. (2017). Competition between precipitation and dissolution in Cu-Ag alloys under high pressure torsion. *Acta Materialia, 122,* 60–71. DOI 10.1016/j.actamat.2016.09.024.
6. Jamal, A. A., Adi, R. A., Rami, A. H. (2019). Use of aluminum alloy plates as externally bonded shear reinforcement for R/C beams. *Procedia Structural Integrity, 17(5),* 403–410. DOI 10.1016/j.prostr.2019.08.053.
7. Zhang, C. H., Song, G. D., Wang, J. (2020). Influence of surface nanocrystallization on aluminizing behavior of AZ91D magnesium alloy. *Rare Metal Materials and Engineering, 49(2),* 0447–0453.
8. Zhang, W., Tian, L. (2014). Experimental study on fatigue property of ZK60 high-strength Mg alloy treated by shot peening. *Hot Working Technology, 43(6),* 153–155.
9. Liu, L., Yu, P. (2020). Design and experiment-based optimization of high-flow hydraulic one-way valves. *Fluid Dynamics & Materials Processing, 16(2),* 211–224. DOI 10.32604/fdmp.2020.08168.
10. Takakuwa, O., Takeo, F., Sato, M., Soyama, H. (2016). Using cavitation peening to enhance the fatigue strength of duralumin plate containing a hole with rounded edges. *Surface and Coatings Technology, 307,* 200–205. DOI 10.1016/j.surfcoat.2016.08.087.
11. Taleyarkhan, R. P., Lapinskas, J., Xu, Y., Cho, J. S., Block, R. C. et al. (2008). Modeling, analysis and prediction of neutron mission spectra from acoustic cavitation bubble fusion experiments. *Nuclear Engineering and Design, 238(10),* 2779–2791. DOI 10.1016/j.nucengdes.2008.06.007.
12. Soyama, H. (2004). Introduction of compressive residual stress using a cavitating jet in air. *Journal of Engineering Materials and Technology, 126(1),* 123–128. DOI 10.1115/1.1631434.
13. Orthaber, U., Petkovšek, R., Schille, J., Hartwig, L., Hawlina, G. et al. (2014). Effect of laser-induced cavitation bubble on a thin elastic membrane. *Optics & Laser Technology, 64(64),* 94–100. DOI 10.1016/j.optlastec.2014.05.008.

14. Soyama, H., Takeo, F. (2016). Comparison between cavitation peening and shot peening for extending the fatigue life of a duralumin plate with a hole. *Journal of Materials Processing Technology, 227,* 80–87. DOI 10.1016/j.jmatprotec.2015.08.012.
15. https://srdata.nist.gov/xps/Default.aspx.
16. Wu, C. L., Wang, B. B., Tao, R., Fang, L. W., Li, H. X. (2018). Study of mineral structure transformation of coal ash with high ash melting temperature by XPS. *Spectroscopy and Spectral Analysis, 38(7),* 2296–2301.